Velocity gradient prediction using parameterized Lagrangian deformation models

Criston Hyett, Yifeng Tian, Michael Woodward, Misha Stepanov, Chris Fryer, Michael Chertkov, Daniel Livescu

July 30, 2023

Abstract

We seek to efficiently predict the statistical evolution of the velocity gradient tensor (VGT) by creating local models for the pressure Hessian. Previous work has identified physics-informed machine learning (PIML) to be adept in this prediction; of note in this class of models is the Tensor Basis Neural Network (TBNN) for its embedded physical constraints and demonstrated performance. Simultaneously, phenomenological models were advanced by approximating the local closure to the pressure Hessian via deformation models using the history of the VGT. The latest in this series of models is the Recent Deformation of Gaussian Fields (RDGF) model. In this work, we combine the (local in time) PIML approach with the phenomenological idea of inclusion of recent deformation to create a data-driven Lagrangian deformation model. We compare the model performance to both the TBNN and the RDGF models, and provide data-driven hypotheses regarding the upstream assumptions made in the RDGF model.

1 Introduction

The velocity gradient tensor (VGT) describes many important aspects of turbulence. It displays characteristic non-Gaussian statistics including intermittency, describes the deformation rate of a fluid volume, and contains encapsulates alignment between strain and vorticity [27]. The VGT has been the subject of much study, and with the exponential growth of compuational power, direct numerical simulations that resolve the smallest scales of turbulence have provided enormous VGT datasets. Even more recently, machine learning (ML), particularly physics-informed machine learning (PIML), have shown remarkable ability to glean predictive capability from these large datasets, suggesting patterns exist that we have not recognized yet.

Of particular note in recent years is recent deformation of Gaussian fields (RDGF) [22], wherein the authors postulate a closure of the VGT evolution equations via choosing a Gaussian upstream condition that is deformed according to the current VGT. This hypothesis is along the same lines as the authors' attempt to close the equations using deformation of a small fluid element [6], but taken to the limit of small time and space.

In the realm of machine learning, the work is inspired by Tian et.al[41], that used a highly structured, so-called tensor basis neural network architecture to close the equations. This network structure was inspired by theoretical work by [25], [22], [31].

Our goals in this paper are to advance the phenomenology via data analysis, and leverage this to improve the TBNN methodology to better predict the statistical evolution of the VGT.

2 Previous Work

2.1 Governing Equations for VGT

Navier-Stokes defines the evolution of a velocity field given a pressure field

$$\frac{\partial u_i}{\partial t} + u_k \frac{\partial u_i}{\partial x_k} = -\frac{\partial P}{\partial x_i} + \nu \frac{\partial^2 u_i}{\partial x_k \partial x_k} \tag{1}$$

The VGT is defined by $A_{ij} = \frac{\partial u_i}{\partial x_j}$, so we apply spatial derivatives to eq(1), and use the definition of material derivative to obtain an ODE for the velocity gradient tensor (defined in the Lagrangian frame)

$$\frac{dA_{ij}}{dt} = \frac{\partial A_{ij}}{\partial t} + u_k \frac{\partial A_{ij}}{\partial x_k} = -A_{ik}A_{kj} - \frac{\partial^2 P}{\partial x_i \partial x_j} + \nu \frac{\partial^2 A_{ij}}{\partial x_k \partial x_k} \tag{2}$$

Using the incompressibility condition,

$$\nabla \cdot u = 0 \implies A_{ii} = 0 \tag{3}$$

we can take the trace of eq(2) to find

$$\frac{\partial^2 P}{\partial x_k \partial x_k} = -A_{ij}A_{ji} \tag{4}$$

which determines the trace of the pressure Hessian. Thus, we can define the so-called deviatoric pressure Hessian as

$$H_{ij} := -\left(\frac{\partial^2 P}{\partial x_i \partial x_j} - \frac{1}{3} \frac{\partial P}{\partial x_k \partial x_k} \delta_{ij} \right) \tag{5}$$

Viellefosse [42] and Cantwell [3] studied the purely local "Restricted Euler" dynamics:

$$E_{ij} := -\left(A_{ik}A_{kj} - \frac{1}{3} A_{mn}A_{nm}\delta_{ij} \right) \tag{6}$$

Finally, letting the viscous term be denoted by

$$T_{ij} := \nu \frac{\partial^2 A_{ij}}{\partial x_k \partial x_k} \tag{7}$$

We can write the ODE for the Lagrangian VGT as

$$\frac{dA_{ij}}{dt} = E_{ij} + H_{ij} + T_{ij} \tag{8}$$

Via numerical studies, the main challenge is to predict the deviatoric pressure Hessian.

2.2 Tensor Basis Neural Network

We can write the formal (nonlocal) solution for the deviatoric pressure hessian as[29]

$$H_{ij}(\mathbf{x}) = \iiint \frac{\delta_{ij} - \hat{r_i}\hat{r_j}}{2\pi r^3} Q(\mathbf{x}+\mathbf{r}) d\mathbf{r} \tag{9}$$

The challenge then, is to obtain an approximation of this nonlocal integral using only local information.

Following Lawson & Dawson[25], an expansion of the integral is proposed, first as a Taylor series expansion in $Q(x+r)$

$$\hat{H} = \sum_{m,n=0}^{\infty} \alpha_{mn} S^m W^n \tag{10}$$

where

$$S = \frac{1}{2}(A + A^T) \qquad W = \frac{1}{2}(A - A^T) \tag{11}$$

Finally we can reduce from an infinite sum using Cayley-Hamilton, and expand via the tensor basis[44],[31]

$$\hat{H} = \sum_{n=1}^{10} g^{(n)}(\lambda_1, \ldots, \lambda_5) T^{(n)} \tag{12}$$

with $g^{(n)}$ scalar functions of the invariants

$$\lambda_1 = \mathrm{tr}(S^2) \quad \lambda_2 = \mathrm{tr}(W^2) \quad \lambda_3 = \mathrm{tr}(S^3) \quad \lambda_4 = \mathrm{tr}(W^2 S) \quad \lambda_5 = \mathrm{tr}(W^2 S^2) \tag{13}$$

and the tensor basis given by:

$$T^{(1)} = S \qquad T^{(2)} = SW - WS \tag{14}$$

$$T^{(3)} = S^2 - \frac{1}{3} I \cdot \mathrm{tr}(S^2) \qquad T^{(4)} = W^2 - \frac{1}{3} I \cdot \mathrm{tr}(W^2) \tag{15}$$

$$T^{(5)} = WS^2 - S^2 W \qquad T^{(6)} = W^2 S + SW^2 - \frac{2}{3} I \cdot \mathrm{tr}(SW^2) \tag{16}$$

$$T^{(7)} = WSW^2 - W^2 SW \qquad T^{(8)} = SWS^2 - S^2 WS \tag{17}$$

$$T^{(9)} = W^2 S^2 + S^2 W^2 - \frac{2}{3} I \cdot \mathrm{tr}(S^2 W^2) \quad T^{(10)} = WS^2 W^2 - W^2 S^2 W \tag{18}$$

This formulation reduces the challenge to finding the functions of known scalars, i.e., learning the $g^{(n)}$'s as shown in fig(1).

This network architecture ensures the output tensor $\hat{H}$ is symmetric, traceless, and the network itself is rotationally and Galilean invariant.

Tian et.al[41] showed ability to train the network, and demonstrated state-of-the-art performance on a variety of relevant physical metrics: eigenvector alignments, Q-R conditional mean tangents (CMTs), *a posteriori* tests evolving an initially Gaussian distributed VGT field to fully developed turbulence as evidenced by characteristic teardrop-shaped Q-R probability distributions (PDFs).

In particular, Tian et.al used

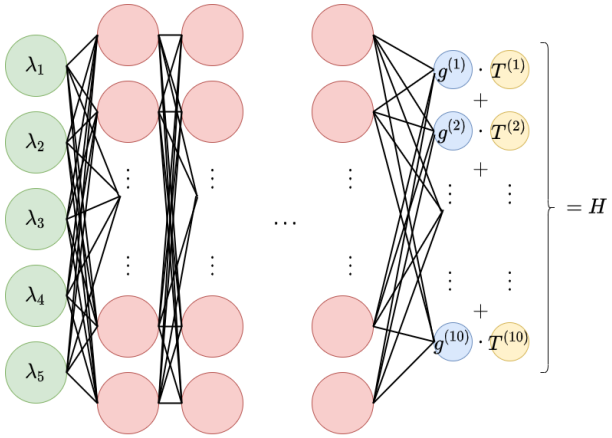

Figure 1: The architecture of the TBNN. The invariants and tensor basis elements are calculated from each sample of the VGT, the invariants are then used as input to a fully connected network, and the resulting $g^{(i)}$ multiply the corresponding tensor basis elements $T^{(i)}$, before summing into the prediction $\hat{H}$

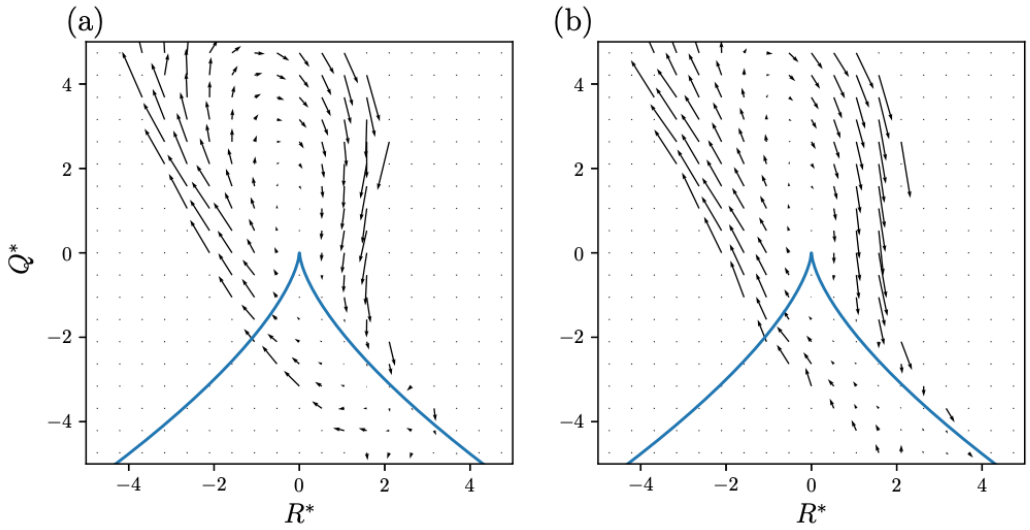

Figure 2: Results from Tian et.al[41] showing Q-R CMTs from (a) DNS data and (b) trained TBNN

2.3 Recent Deformation of Gaussian Fields

A note on notation in this section - I use the notation of Johnson & Meneveau as I am explaining their model, and they mean something specific by using it. Throughout the rest of the paper, the idea is however much the same, e.g., a neural network attempts to make the best approximation of the expected pressure Hessian, conditioned upon samples. Thus the change in notation is largely artificial here.

Johnson and Meneveau[22] introduced the RDGF model following a long line of postulating that the deviatoric part of the pressure Hessian could be locally modeled using information of the time history of the deformation tensor [6],[8],[7].

Chertkov et.al's Tetrad Model, attempted to capture this deformation directly by following a small fluid element approximated by 4 Lagrangian particles. This model avoided the finite time singularity resulting from using only the restricted Euler term[3], and attempts to fuse this low-dimensional model of a fluid element with data-driven methods for prediction of the coarse-grained VGT are ongoing[17],[16]. Chevillard & Meneveau used the same initially isotropic upstream condition as in the Tetrad Model when developing their Recent Fluid Deformation (RFD) model. Finally, Johnson & Meneveau enriched the approximation of the upstream condition using high fidelity direct numerical simulation (DNS) data[43].

RDGF models the conditional average of the pressure Hessian as

$$\langle P_{ij}|A\rangle = \left\langle \frac{\partial^2 p}{\partial x_i \partial x_j}|A \right\rangle = \frac{\partial X_k}{\partial x_i}\left\langle \frac{\partial^2 p}{\partial X_k \partial X_l}|A \right\rangle \frac{\partial X_l}{\partial x_j} = D^{-1}_{ki}\langle \tilde{P}_{kl}|A\rangle D^{-1}_{lj} \tag{19}$$

Where $\tilde{P_{kl}}$ is an upstream pressure Hessian, and the deformation tensor is given by

$$D_{ij} = \frac{\partial x_i}{\partial X_j} \tag{20}$$

and evolves according to (assuming isotropic initial condition - this is without loss of generality for sufficiently far removed upstream times)

$$\frac{dD_{ij}}{dt} = A_{ik}D_{kj} \quad \text{with } D_{ij}(0) = \delta_{ij} \tag{21}$$

so that the general solution is defined via the time-ordered exponential

$$D_{ij}(t) = \mathrm{Texp}(A(t)) = \lim_{N\to\infty}\prod_{i=0}^{N}\left(e^{A(t_i)\Delta t}\right) \tag{22}$$

where the product is the left product, and $t_0 = 0, t_N = t$. If we take the leading order term, we get the RDGF approximation

$$D(x,t) \approx \exp\left[A(x,t)\Delta t\right] \tag{23}$$

The upstream pressure Hessian is given by

$$\langle \tilde{P}_{ij}|A\rangle \approx \frac{1}{3}\langle \tilde{P}_{kk}|A\rangle\delta_{ij} + \langle \tilde{P}^{(d)}_{ij}|A\rangle_{\text{Gaussian}} \tag{24}$$

where, using the notation of the tensor basis, eqs(14-18)

$$\langle \tilde{P}^{(d)}_{ij}|A\rangle_{\text{Gaussian}} = \gamma T^{(2)} + \alpha T^{(3)} + \beta T^{(4)} \tag{25}$$

with the coefficients

$$\alpha = -\frac{2}{7}, \quad \beta = -\frac{2}{5}, \quad \gamma \approx 0.08 \tag{26}$$

By enforcing the prediction eq(24) to have trace of $2Q$, and labeling

$$G_{ij} := D_{mi}^{-1} \langle \tilde{P}_{ij}^{(d)} | A \rangle_{\text{Gaussian}} \tag{27}$$

The prediction of the pressure Hessian becomes

$$\langle P_{ij} | A \rangle = 2Q \frac{C_{ij}^{-1}}{C_{kk}^{-1}} + G_{ij} - \frac{C_{ij}^{-1}}{C_{kk}^{-1}} G_{ll} \tag{28}$$

3 Methodology

This section is a work-in-progress. I talk more about this in the prospectus, and welcome comments and ideas.

3.1 Proposed Models

Our approach is to utilize the idea of biasing the statistics of the conditional deviatoric pressure Hessian using the history of the VGT (as in the RDGF, RFD, and Tetrad models), while avoiding postulating the exact functional form; instead allowing it to be data-driven using PIML (as in TBNN model).

We do this by augmenting the inputs to the feed-forward portion of the TBNN, the idea being to bias the statistics of the invariants, while believing that the tensors derived from the local-in-time VGT are sufficient to span the function space.

3.1.1 Temporal Convolution

The simplest of our proposed models augments the set of invariants using a learned temporal convolution.

$$\hat{H} = \sum_{n=1}^{10} g_\theta^{(n)}(\lambda_1, \ldots, \lambda_5, X) T^{(n)} \tag{29}$$

with

$$X(t) = \sum_{t_f}^{t_f - \Delta t \cdot n} \zeta_n A_n \tag{30}$$

where ζ_n are learned simultaneously with the parameterization of the scalar g functions.

This model avoids biasing the prediction with phenomenological thoery, but at the cost of computational overhead. However, because of the simple structure, the learned ζ's may inform a temporal correlation in the VGT that is useful in the prediction of the deviatoric pressure Hessian. An extreme case of very short time correlations would reinforce the hypothesis presented in RDGF, while longer temporal correlations would support the modeling approaches of e.g., [40].

3.1.2 Time-Ordered Exponential

Finally, we may take an intermediate step between the two, and introduce the time-ordered exponential to the network, setting

$$X(t) = \text{Texp}[A] \tag{31}$$

in eq(29)

3.2 Data Analysis

In this section we perform numerical studies on DNS data to evaluate assumptions and choices for model hyperparameters.

3.2.1 Ground Truth Data

Our data is DNS of forced isotropic turbulence with $Re = 240$. Eularian data is generated, random points are sampled, VGT and pressure Hessian are constructed at these points using interpolation, and Lagrangian trajectories of these quantities are advanced using the Eularian velocity fields. We have 122k samples, each advanced for 1000 timesteps with $\Delta t = 3e - 4$, representing approximately half an inertial eddy turnover time. For each sample and each timestep, we have measured VGT, PH, and viscous terms.

3.2.2 Cramer Functions of Strain Rate Eigenvalues

Coarsely stated, the Cramer function (also more generally called the rate function) determines how quickly large deviations from a mean diminish. If we believe in the ability to close the equations for the deviatoric pressure Hessian locally, it is apparent that there must exist a relation between temporal correlations of the strain-rate tensor, and temporal correlations of the deviatoric pressure Hessian.

3.2.3 Gaussian Upstream Condition

The Gaussian upstream condition present in RDGF is convenient, but for short deformation time is known to be inaccurate. Via analysis of Lagrangian data, we can evaluate how long the deformation time must be to transform the Gaussian upstream condition to a distribution representative of fully developed turbulence. In particular, we can evaluate

$$\min_{\Delta t} \left\| P_{gt}^{(d)} - P'^{(d)}_{\text{Gaussian}}(\Delta t) \right\| \tag{32}$$

where $P'^{(d)}_{\text{Gaussian}}(\Delta t)$ is the true deformation of the Gaussian upstream condition, by the ground truth VGT over a time Δt.

4 Results

4.1 Hyperparameter Tuning

One important deviation from the guiding paper is in data normalization. Tian et.al, normalized the VGT and PH using an empirical measure of the timescale

$$\tau \approx \langle \left\| S^2 \right\| \rangle^{-1} \tag{33}$$

In our work, we confirmed it was vital to performance to normalize the VGT

$$A' = \tau A \tag{34}$$

but found the network performance suffered considerably if the PH was normalized. One hypothesis is that this is an artifact of initialization of the network parameters. The PH should be normalized by τ^2, which for $Re = 240$ $\tau \approx 3e-3$. If one uses this normalization, the network does train, but it seems to start very far away from the optimal. It is possible this could remedied by scaling the initialization of the linear output layer as well as individualizing that layer's learning rate - this was not performed.

In calculation of the $g^{(i)}$ functions, we use a fully connected feed-forward network with 5 hidden layers of 50 nodes apiece with relu activation functions and a linear output layer. This network is trained using the ADAM optimizer with learning rate $5e-3$ decaying to a minimum of $1e-6$ via factors of 2 when the loss reaches a plateau.

4.2 Result reproduction

After implementing this network architecture and finding the hyperparameters above, the results in figure(3) were found. These results agree well with the original paper, and suggest the hyperparameter choices were accurate.

4.3 Temporal Convolution TBNN

Preliminary results suggest that the additional historical information of the VGT is in fact useful for the prediction of the PH. In figure(4), results of training the temporal convolution TBNN (convTBNN) are shown, improving both in the loss and eigenvector alignment metrics.

An interesting aspect of the convTBNN is the ability to inspect the kernel length - loosely the length over which the network found it useful to set weights away from zero. Figure(5) displays the weights as a function of kernel entry number. The sampling in time occurs every $20\Delta t$, where $\Delta t = 3e-4$ and the Kolmogorov timescale is $\tau \approx 3e-3$, so that the sampling occurs about every 2τ. We see that only the last three weights are nonzero, suggesting that a history of about 6τ is useful in prediction.

5 Conclusion

In this work (in progress), we reproduced the current state-of-the-art Lagrangian model to predict the PH, contextualized it with recent phenomenological advancements, and advanced the methodology by introducing and evaluating a new predictive model.

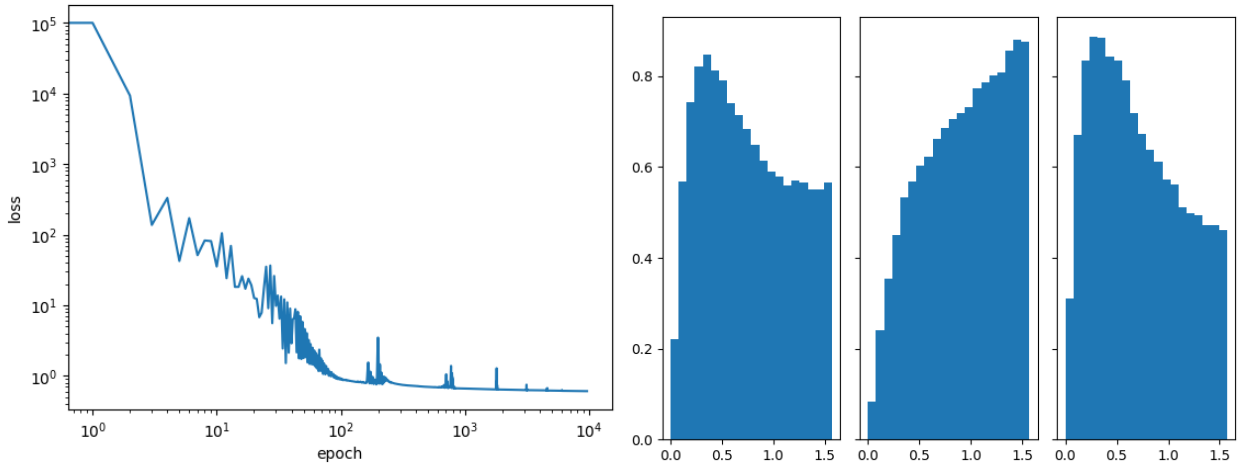

Figure 3: (left) Loss as a function of epoch for the TBNN, (right) PDFs of eigenvalue alignment for the pressure hessian, sorted from smallest to largest eigenvalue left to right. These plots agree well with results from Tian et.al's paper, suggesting the implementation is correct.

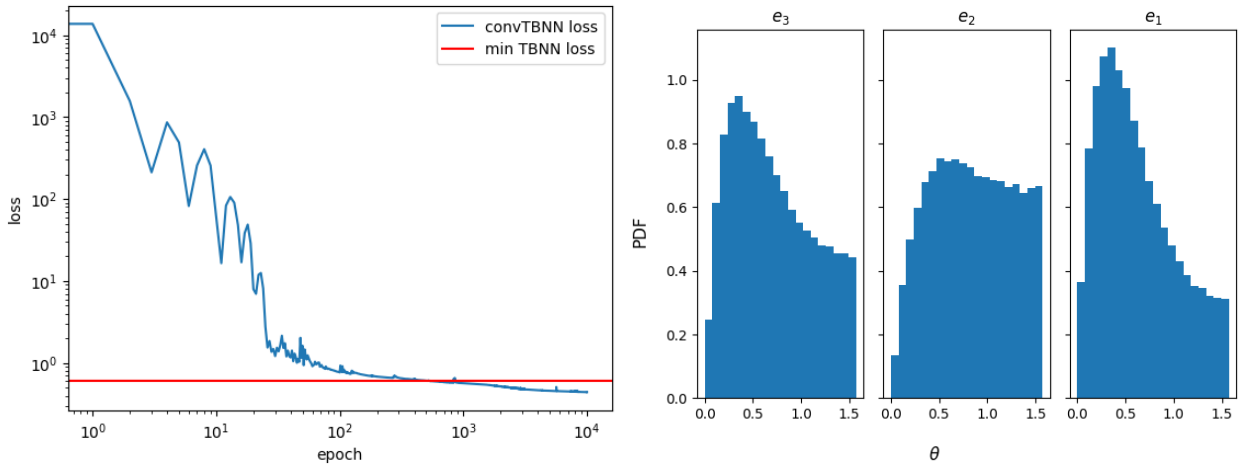

Figure 4: Preliminary results of training the convTBNN. (Left) shows the loss vs epoch, with the minimum loss obtained by the unmodified TBNN marked in horizontal red, and the convTBNN in blue. (Right) shows the alignment PDFs of eigenvectors of the PH. Here e_1 corresponds to the eigenvector with the greatest associated eigenvalue. Note that compared to fig(3), all alignment PDFs are better, shifting significant density from the misaligned (larger θ) to aligned.

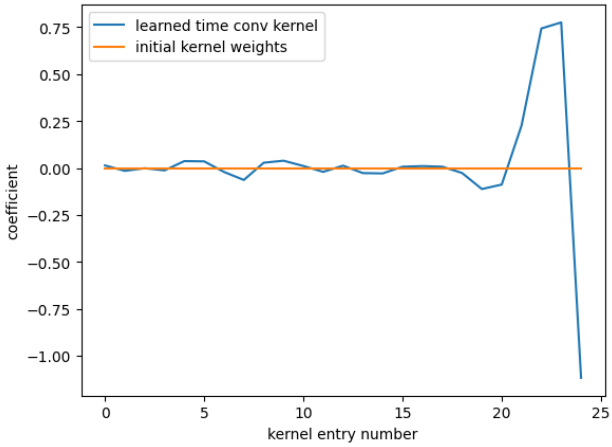

Figure 5: The weights of the learned temporal convolution kernel. This may act as a stand-in for a measure of significance for VGT history as it relates to the prediction of the PH. If these results hold across many trainings, it would suggest that only "recent" history is informative in prediction of the PH.

The TBNN is a powerful tool to capture symmetries, while allowing for the flexibility of a NN. We applied this model to homogeneous, isotropic turbulence to close the equations of the non-local pressure Hessian using only the local velocity gradient tensor. We contrasted this approach with a mathematically similar, but philosophically different approach using the RDGF model, motivated by the idea that the recent history of the VGT could better inform the prediction of the current PH.

By combining the two, we created the convTBNN, a first data-driven step towards biasing the statistics of the current PH prediction using the history of the VGT. We showed that we could outperform the local in time TBNN in two metrics, loss value and eigenvector alignment. We began to interpret the weights of the temporal convolution kernel, and related them to the hypotheses made in the phenomenological models (RFD, RDGF).

Further work needs to be done to ensure these results hold under evaluation of richer metrics such as the Q-R conditional mean tangents, and evaluate the accuracy and stability of the resulting differential equation for the VGT.

6 Appendix

6.1 Interpretability

Previous work by the authors [18] suggested there may be a latent space in the invariants when predicting the PH using the TBNN. The existence of a latent space could be important to the ability to interpret the results, e.g. searching for a functional form or providing physical insight; or if we believe in the statistical independence of the input (in our case there are many reasons to) it suggests the network struggles to exploit the additional information. In the case of [18] it seems to be the latter.

The proposed latent space is indeed persistent when training the network having normalized the PH using τ^2, in particular, the latent space claimed consists only of

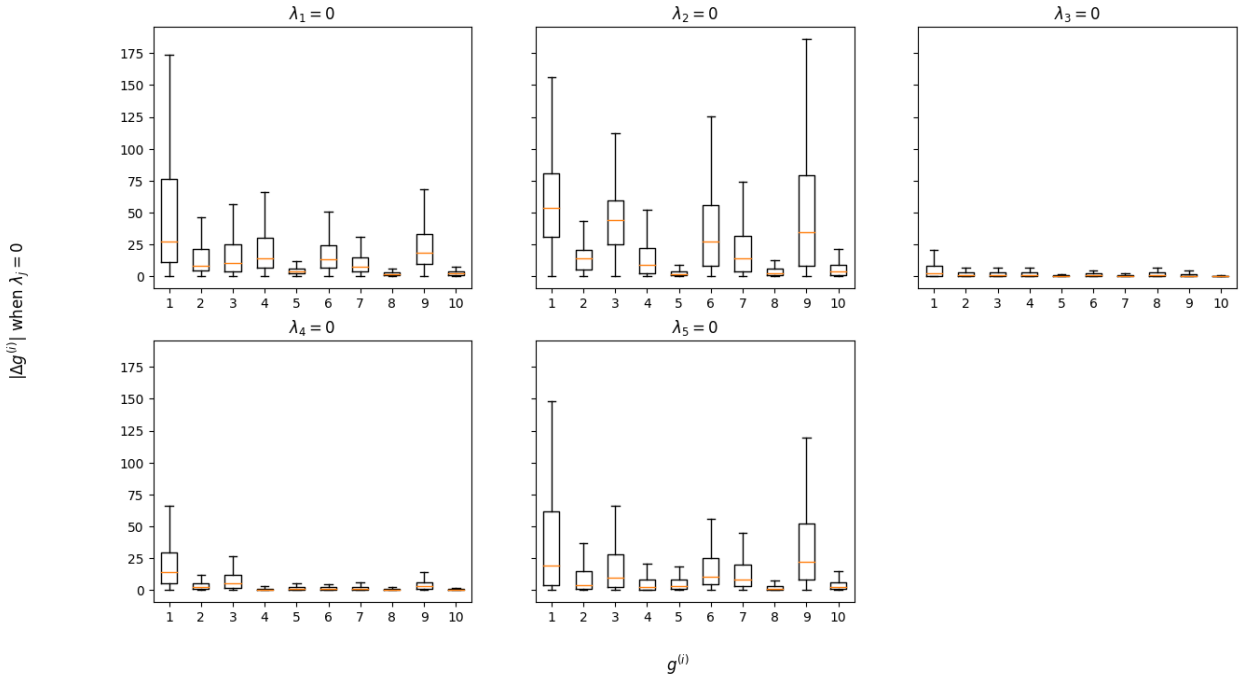

Figure 6: Distributions of sensitivity of $g^{(i)}$ to variability of λ_j. Previous work performed suggested that λ_{3-5} were unimportant to the prediction using the TBNN. This result was predicated upon the normalization of the PH using τ^2. While our plot reinforces that $\lambda_{3,4}$ do provide an order of magnitude smaller correction, the sensitivity of the network to λ_5 is of the same order of magnitude as that to $\lambda_{1,2}$. This suggests that by *not* normalizing the PH, we are able to exploit additional information in the invariants.

the low-order invariants. The hypothesis by the author was that the latent space emerged as a numerical artifact of strong normalization of the high-order invariants ($\lambda_{3,4} \to \tau^3\lambda_{3,4}$, and $\lambda_5 \to \tau^4\lambda_5$). But as we show in figure(6), there exists leading-order sensitivity to λ_5 (and not insignficant sensitivity to $\lambda_{3,4}$) when the PH is *not* normalized. This may indicate that the low-order latent space was a numerical artifact resulting from very small weights in the *output layer*, combined with strong normalization of high-order invariants.

To explore this question further, we applied an autoencoder to the set of invariants, as well as calculated the mutual information between the invariants.

The mutual information calculation, shown in table(1), indicates that while the invariants are not strictly independent, they are also far from highly correlated. The maximum value - biased away from the ideal value of 10 here by the k-nearest neighbors algorithm with $k = 5$, detailed in [35].

The autoencoder structure is a fully connected, feed forward neural network,

$$AE_\theta : \mathbb{R}^5 \to \mathbb{R}^5 \text{ via } \mathbb{R}^5 \to \mathbb{R}^4 \to \mathbb{R}^h \to \mathbb{R}^4 \to \mathbb{R}^5 \tag{35}$$

where h is the imposed latent dimension, illustrated in fig[7]. The nonlinear activation functions of AE_θ are the so-called "leaky-relu". We implement the "robust max-min" normalization, relying on the interquartile distance - namely, letting Q_1, Q_3 be the first

$I(\lambda_i, \lambda_j)$	λ_1	λ_2	λ_3	λ_4	λ_5
λ_1		0.26350727	1.40593169	0.40473788	0.72127464
λ_2			0.1968969	0.80102301	0.95679744
λ_3				0.43549834	0.49519878
λ_4					0.83990126
λ_5					

Table 1: A scaled mutual information $I(\lambda_i, \lambda_j)$, between invariants. Note the maximum value is near 10, the method used here introduces a bias however, namely via k-nearest neighbors with $k = 5$, as discussed in [35]

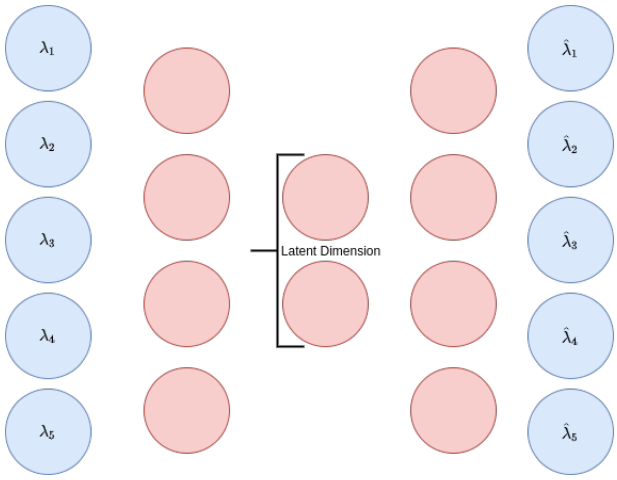

Figure 7: Autoencoder structure applied to the invariant input data.

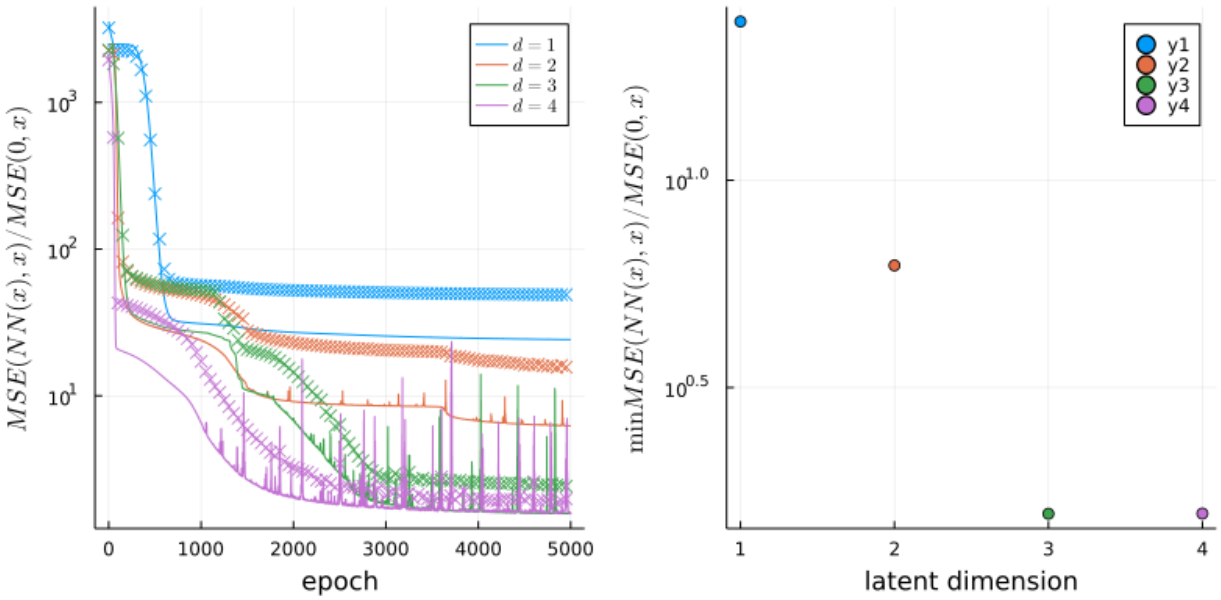

Figure 8: Autoencoder applied to the invariant input data, in an attempt for a nonlinear projection onto a latent space. (Left) shows the evolution of the loss according to the imposed latent dimension, where 'x's mark test loss, while solid lines mark training loss. (Right) shows the minimum loss as a function of latent dimension. Notice the two jumps at $h = 2$ and $h = 3$ - suggesting a sequence of increasing fidelity.

and third quartiles, we normalize our invariants as

$$\tilde{\lambda_i} = \frac{\lambda - Q_1}{Q_3 - Q_1} \tag{36}$$

This is intentionally different than the normalization used in the TBNN, as normalizing via timescale and optimizing using the mean-squared-error gives a very strong preference towards reconstructing only the low-order invariants. The robust max-min normalization is an attempt to set each on an equal footing, but itself is subject to biases introduced by differences in distribution shapes.

We use the ADAM optimizer with learning rate $\eta = 1e-3$, partitioning the dataset of 100k samples into 75% training, 25% test. The results are shown in fig[8] and may suggest a small reduction in dimension (i.e., $5 \to 3$). These results match the leading order contributions to the sensitivities of the $g^{(i)}$ as shown in fig(6), but we caution this suggestion as the low-order basis elements are still significantly influenced.

References

[1] Wm. T. Ashurst, A. R. Kerstein, R. M. Kerr, and C. H. Gibson. Alignment of vorticity and scalar gradient with strain rate in simulated navier–stokes turbulence. *The Physics of Fluids*, 30(8):2343–2353, 1987.

[2] R. Betchov. An inequality concerning the production of vorticity in isotropic turbulence. *Journal of Fluid Mechanics*, 1(5):497–504, 1956.

[3] Brian J. Cantwell. Exact solution of a restricted euler equation for the velocity gradient tensor. *Physics of Fluids A: Fluid Dynamics*, 4(4):782–793, 1992.

[4] Tian Qi Chen, Yulia Rubanova, Jesse Bettencourt, and David Duvenaud. Neural ordinary differential equations. *CoRR*, abs/1806.07366, 2018.

[5] M. Chertkov, G. Falkovich, I. Kolokolov, and V. Lebedev. Normal and anomalous scaling of the fourth-order correlation function of a randomly advected passive scalar. *Phys. Rev. E*, 52:4924–4941, Nov 1995.

[6] Michael Chertkov, Alain Pumir, and Boris I. Shraiman. Lagrangian tetrad dynamics and the phenomenology of turbulence. *Physics of Fluids*, 11(8):2394–2410, 1999.

[7] L Chevillard, C Meneveau, L Biferale, and F Toschi. Modeling the pressure hessian and viscous laplacian in turbulence: comparisons with direct numerical simulation and implications on velocity gradient dynamics. *Physics of Fluids*, 20(10), 2008.

[8] Laurent Chevillard and Charles Meneveau. Lagrangian dynamics and statistical geometric structure of turbulence. *Physical review letters*, 97(17):174501, 2006.

[9] M. S. Chong, A. E. Perry, and B. J. Cantwell. A general classification of three-dimensional flow fields. *Physics of Fluids A: Fluid Dynamics*, 2(5):765–777, 1990.

[10] Mohammad Danish and Charles Meneveau. Multiscale analysis of the invariants of the velocity gradient tensor in isotropic turbulence. *Phys. Rev. Fluids*, 3:044604, Apr 2018.

[11] Rishita Das and Sharath S. Girimaji. On the reynolds number dependence of velocity-gradient structure and dynamics. *Journal of Fluid Mechanics*, 861:163–179, 2019.

[12] Rishita Das and Sharath S. Girimaji. Characterization of velocity-gradient dynamics in incompressible turbulence using local streamline geometry. *Journal of Fluid Mechanics*, 895:A5, 2020.

[13] D. A. Donzis, P. K. Yeung, and K. R. Sreenivasan. Dissipation and enstrophy in isotropic turbulence: Resolution effects and scaling in direct numerical simulations. *Physics of Fluids*, 20(4):045108, 2008.

[14] Adrienne L. Fairhall, Barak Galanti, Victor S. L'vov, and Itamar Procaccia. Direct numerical simulations of the kraichnan model: Scaling exponents and fusion rules. *Phys. Rev. Lett.*, 79:4166–4169, Nov 1997.

[15] G. Falkovich, K. Gawędzki, and M. Vergassola. Particles and fields in fluid turbulence. *Rev. Mod. Phys.*, 73:913–975, Nov 2001.

[16] Criston Hyett, Michael Chertkov, Yifeng Tian, and Daniel Livescu. Machine learning statistical lagrangian geometry of turbulence. In *APS Division of Fluid Dynamics Meeting Abstracts*, pages S01–024, 2020.

[17] Criston Hyett, Michael Chertkov, Yifeng Tian, Daniel Livescu, and Mikhail Stepanov. Machine learning statistical evolution of the coarse-grained velocity gradient tensor. In *APS Division of Fluid Dynamics Meeting Abstracts*, pages E31–009, 2021.

[18] Criston Hyett, Yifeng Tian, Michael Woodward, Michael Chertkov, Daniel Livescu, and Mikhail Stepanov. Applicability of machine learning methodologies

to model the statistical evolution of the coarse-grained velocity gradient tensor. *Bulletin of the American Physical Society*, 2022.

[19] Michael Innes, Elliot Saba, Keno Fischer, Dhairya Gandhi, Marco Concetto Rudilosso, Neethu Mariya Joy, Tejan Karmali, Avik Pal, and Viral Shah. Fashionable modelling with flux. *CoRR*, abs/1811.01457, 2018.

[20] Mike Innes. Flux: Elegant machine learning with julia. *Journal of Open Source Software*, 2018.

[21] Perry L. Johnson and Charles Meneveau. Large-deviation joint statistics of the finite-time lyapunov spectrum in isotropic turbulence. *Physics of Fluids*, 27(8):085110, 2015.

[22] Perry L. Johnson and Charles Meneveau. A closure for lagrangian velocity gradient evolution in turbulence using recent-deformation mapping of initially gaussian fields. *Journal of Fluid Mechanics*, 804:387–419, 2016.

[23] Perry L. Johnson and Charles Meneveau. Turbulence intermittency in a multiple-time-scale navier-stokes-based reduced model. *Phys. Rev. Fluids*, 2:072601, Jul 2017.

[24] Robert H. Kraichnan. Convection of a passive scalar by a quasi-uniform random straining field. *Journal of Fluid Mechanics*, 64(4):737–762, 1974.

[25] J. M. Lawson and J. R. Dawson. On velocity gradient dynamics and turbulent structure. *Journal of Fluid Mechanics*, 780:60–98, 2015.

[26] Thomas S. Lund and Michael M. Rogers. An improved measure of strain state probability in turbulent flows. *Physics of Fluids*, 6(5):1838–1847, 1994.

[27] Charles Meneveau. Lagrangian dynamics and models of the velocity gradient tensor in turbulent flows. *Annual Review of Fluid Mechanics*, 43:219–245, 2011.

[28] Parviz Moin and Krishnan Mahesh. Direct numerical simulation: A tool in turbulence research. *Annual Review of Fluid Mechanics*, 30(1):539–578, 1998.

[29] Koji Ohkitani and Seigo Kishiba. Nonlocal nature of vortex stretching in an inviscid fluid. *Physics of Fluids*, 7(2):411–421, 1995.

[30] ANDREW OOI, JESUS MARTIN, JULIO SORIA, and M. S. CHONG. A study of the evolution and characteristics of the invariants of the velocity-gradient tensor in isotropic turbulence. *Journal of Fluid Mechanics*, 381:141–174, 1999.

[31] S. B. Pope. A more general effective-viscosity hypothesis. *Journal of Fluid Mechanics*, 72(2):331–340, 1975.

[32] Christopher Rackauckas and Qing Nie. Differentialequations.jl – a performant and feature-rich ecosystem for solving differential equations in julia. *The Journal of Open Research Software*, 5(1), 2017. Exported from https://app.dimensions.ai on 2019/05/05.

[33] Maziar Raissi and George E. Karniadakis. Hidden physics models: Machine learning of nonlinear partial differential equations. *CoRR*, abs/1708.00588, 2017.

[34] Hannes Risken and Frank Till. *The Fokker-Planck Equation*. Springer,Berlin,Heidelberg, 1996.

[35] Brian C Ross. Mutual information between discrete and continuous data sets. *PloS one*, 9(2):e87357, 2014.

[36] A. J. M. Spencer and R. S. Rivlin. Further results in the theory of matrix polynomials. *Arch. Rational Mech. Anal.*, 4:214–230, 1959.

[37] Anthony James Merrill Spencer and Ronald S Rivlin. The theory of matrix polynomials and its application to the mechanics of isotropic continua. *Archive for rational mechanics and analysis*, 2:309–336, 1958.

[38] K. R. Sreenivasan and R. A. Antonia. The phenomenology of small-scale turbulence. *Annual Review of Fluid Mechanics*, 29(1):435–472, 1997.

[39] Hendrik Tennekes and John Leask Lumley. *A first course in turbulence*. MIT press, 1972.

[40] Yifeng Tian, Yen Ting Lin, Marian Anghel, and Daniel Livescu. Data-driven learning of mori–zwanzig operators for isotropic turbulence. *Physics of Fluids*, 33(12):125118, 2021.

[41] Yifeng Tian, Daniel Livescu, and Michael Chertkov. Physics-informed machine learning of the lagrangian dynamics of velocity gradient tensor. *Physical Review Fluids*, 6(9):094607, 2021.

[42] P. Vieillefosse. Internal motion of a small element of fluid in an inviscid flow. *Physica A: Statistical Mechanics and its Applications*, 125(1):150–162, 1984.

[43] M Wan, S Chen, G Eyink, C Meneveau, E Perlman, R Burns, Y Li, A Szalay, and S Hamilton. Johns hopkins turbulence database (jhtdb), 2016.

[44] Q.-S. Zheng. On the representations for isotropic vector-valued, symmetric tensor-valued and skew-symmetric tensor-valued functions. *International Journal of Engineering Science*, 31(7):1013–1024, 1993.

Control of Line Pack in Natural Gas System: Balancing Limited Resources under Uncertainty

Criston Hyett, Laurent Pagnier, Jean Alisse, Lilach Sabban,
Igal Goldshtein and Michael Chertkov
{cmhyett,laurentpagnier,chertkov}@math.arizona.edu,
{Jean.Alisse,Lilah.Saban,Igal.Goldshtein}@noga-iso.co.il

April 5, 2023

Abstract

We build and experiment with a realistic but reduced natural gas model of Israel. The system is unusual because (a) it is controlled from a limited number of points which are at, or close to, the gas extraction sites offshore of Israel's Mediterranean coast; (b) control specifies average flux at inlet, not pressure; (c) there are no inland compressors to regulate pressure; (d) power system is the main consumer of gas (70% of Israel's power is generated at gas-fired power plants distributed across the country). Nature of the system suggests that a special attention should be given to understanding dynamics driven by fast transients in gas consumption meeting intra-day variations in the electricity demand, and accounting for increasing role of uncertain renewable generation (mainly solar). Based on all of the above we pose and resolve a sequence of dynamic and control challenges, such as: How to time ramping up- and down- injection of gas to guarantee a healthy intra-day line-pack which meets both pressure constraints and gas-extraction patterns? We report simulation results and utilize monotonicity properties of the natural gas flows which render robustness of our conclusions to the uncertainties of the edge withdrawals of gas.

1 Introduction

This is the first manuscript of the joint NOGA (Power System Operator of Israel) and UArizona team. We aim in this manuscript

- To explain specifics of the Natural Gas system of Israel, describe its minimal model and formulate main operational challenges related to uncertainty in production and consumption, also amplified by limited availability of resources. [Section 2]
- To describe basic modeling tools which allow us to study the system, including description of equations and of the software utilized. [Section 3]
- To formulate operational scenarios, reflecting the aforementioned uncertainty, and present analysis and control solutions. [Section 4]
- To sketch further plans to extend the demonstrated methodologies towards (a) joint, and thus more realistic, modeling and control of natural gas and power systems of Israel; but also (b) formulating further practical and academic challenges towards exporting the developed methodology to other energy systems of the size comparable to the one of Israel. [Section 6.]

2 Motivation, Data & Sources

Following the signing of the global agreement at the Paris Climate Conference in 2015, Israel set long-term goals to reduce greenhouse gas emissions in an effort to take part in the global action against climate change. Since the discovery of substantial offshore gas fields off the coast of Israel, Natural Gas (NG) has become the main fuel for electricity production in the country. In order to reduce Israel's carbon footprint, a decision has been made to close both major coal-fueled power plants at Hadera and Ashkelon in the future, and to convert them to gas fueled units. Apart from renewable energy, this will render NG as the sole source of energy for electricity in the country. The Ministry of Energy plan is aimed at fulfilling Israel's role in the agreement and at promoting an efficient, green economy. The objective is to generate up to 30% of electricity using renewable energy by 2030, and potentially generate up to 100% of electricity this way by 2050. The increasing share of renewable energy presents several challenges in the interim however, particularly with regard to the effects on the natural gas system, which must balance the intermittent and variable electricity production of uncontrollable renewable sources.

As of 2020, more than 50% of Israel's electricity is produced from NG. The yearly demand for NG recently increased beyond 11 billion cubic meters (BCM). During the transition to the 2030 goal, that share is expected to increase up to 80%-85% in certain years. Moreover, two agreements were signed with Egypt and Jordan stipulating that Israel will export 130 BCM of NG from the Leviathan and Tamar gas fields over the next ten years. (At the moment, the non-electricity end use of NG in Israel is small, amounting to around 9000 MMBTU/h or around 10% of the hourly typical flow). Those data show that there are many issues surrounding the NG network in Israel over the next decade.

NOGA, Israel Independent System Operator (IISO), is the newly founded Israeli Electric System Operator. Its mandate is to act to ensure

#	n_s	n_e	L	D
1	1	2	26	600
2	2	3	28.5	600
3	3	4	25	600
4	3	5	56	600
5	5	6	81	445
6	1	7	77	736
7	7	8	22	757
8	8	9	14	743
9	2	9	102	914
10	9	10	34.4	766
11	9	11	34.4	914
12	1	2	26	914
13	2	3	28.5	914

Figure 1: Description of the Israeli gas system: (left) Sketch of the true system. (center) Map of the reduced 11-node system that we use for this study. (right) List of pipelines in the simplified system. Their start node (n_s), end node (n_e), length L in km, and diameter D in mm.

continuous electricity supply, at the required reliability and quality level, to all electricity consumers, in normal and emergency system conditions, and to manage the wholesale electricity market operations competitively and equitably. In addition to managing day-to-date operations, IISO is also in charge for planning development of the generation system, including recommendations for the required generation and storage capacity, maintaining optimal mix, location and timing for integration of generation and storage facilities. IISO is tasked to set up criteria for planning the development of the generation system. The company mandate also includes many other aspects of the transmission system planning, such as related to data forecast, transformer placement and characterization and, overall, formulation of a multi-year plan for the transmission system development. It is recognized, that to achieve all the goals IISO needs state-of-the-art tools to model the Natural Gas system and its interaction with the Electricity network.

In this manuscript we present a reduced, schematic gas model of Israel based on open-source public resources, shown in Figure 1. The data source is the website of the Israel Natural Gas Authority

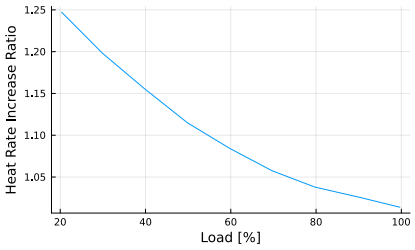

Figure 2: Typical Gas Turbine Efficiency Curve

www.ingl.co.il. In order to perform the simulations, we need to create time series of the gas withdrawals at the model nodes. To do this, we use public data published by the Electricity Authority from the website `https://www.gov.il/he/departments/general/hovatdivuahnetunim`. The data are in the form of half-hourly time series of electricity production (in MW) at all units. We convert the power data to gas consumption with the help of typical gas turbines efficiency curves (see Figure 2 for an example of such a curve).

3 Dynamic Modeling of Pipe Flow

We utilize dynamic modeling discussed in [1, 2, 3] (see also references therein) and specific algorithmic scheme from [4] called GasTranSim.jl implemented by Los Alamos National Laboratory team in Julia [5].

Basic equations, expressing conservation of mass and momentum and describing flow of gas in a single pipe (with gas velocity much smaller than the speed of sound), are [1, 2]:

$$\partial_t \rho + \partial_x \phi = 0, \tag{1}$$

$$\partial_t \phi + \partial_x p = -\frac{\lambda}{2D}\frac{\phi|\phi|}{\rho}, \tag{2}$$

where $\rho(t;x)$, $\phi(t;x)$ and $p(t;x)$ are the gas density, mass flux and pressure measured at the moment of time t at the position x along the pipe; λ is the Darcy-Weisbach friction factor of the pipe (per diameter, D). Eqs. (1) -(2) are supplemented by the equation of state, relating pressure and density

$$p = Z(\rho, T)RT\rho \tag{3}$$

In this study we use the CGNA formula for $Z(\rho, T)$, see e.g. [6]. Effects of gravity and temperature variations along the system are ignored, as the effects are small and our representation is schematic [1].

The single pipe description extends to a system of pipes. Each pipe is characterized by three parameters: diameter, length, and the friction factor per diameter. Each node prescribes a boundary condition for one side of (at-least) one pipe at all instances in time. Additionally, nodes and pipes are joined via condition of mass conservation (Kirchoff's rule, that the mass entering a junction must equal the mass exiting the junction). As is standard, demand nodes specify a flux withdrawal as a function of time. The system in question however, additionally specifies flux at supply nodes. Thus all supplied boundary conditions are on flux.

Denoting ρ_{ij}, ϕ_{ij} to be the dynamic variables on the pipe from node i to node j, and ρ_n, ϕ_n to be the density and flux at node n, we write the

[1] Taking into account the temperature variations is only important in countries with sub-zero winter temperatures. In Israel, this is not the case and we make the assumption of a constant temperature equal to 15 Celsius degrees. Accounting for the effects of elevation/gravity is of a concern only at the node #6, located in the Dead Sea area, roughly 400 meters below the sea level, and at the node # 5, located close to Beer-Sheva at 300 meters above the sea level. Given that ignorning this effect results only in a relatively minor pressure drop of 3 to 5 bars in the southern part of the system, we ignore it for now in the simplest version of the model.

full system to be solved as:

$$\partial_t \rho_{ij} + \partial_x \phi_{ij} = 0 \tag{4}$$

$$\partial_t \phi_{ij} + \partial_x p_{ij} = -\frac{\lambda_{ij}}{2D} \frac{\phi_{ij}|\phi_{ij}|}{\rho_{ij}} \tag{5}$$

subject to initial and boundary conditions:

$$\rho_{ij}(x,0) = \rho_{0,ij}(x) \tag{6}$$

$$\phi_{ij}(x,0) = \phi_{0,ij}(x) \tag{7}$$

$$\phi_n(t) = d_n(t) \tag{8}$$

$$\sum_{j \in \mathcal{E}} \phi_j S_{ij} + d_j = 0 \tag{9}$$

Where S_{ij} is the cross-section of the pipe. Initial conditions for density and mass-flux in the system are constructed based on actual operational data. To solve for dynamics of mass flows and pressures across the system we use the staggered-grid approach of [4] which is an explicit, conservative, second order, finite difference scheme, stable given a CFL condition is satisfied. We remind that, as of now, the Israel system does not contain compressors.

4 Operational Scenarios

We search for robustness in the face of challenging scenarios. To this end we construct scenarios that represent two basic phenomena:

- Moderate uncertainty at demand nodes, represented through addition of a random noise at the consumption site, e.g. associated with response of gas-generators to renewable fluctuations on the electric-side of the system.

  $$d_i(t) \to X_i(t) \tag{10}$$

  where

  $$dX_i(t) = \alpha(d_i(t) - X_i(t)) + \gamma dW \tag{11}$$

  is a Ornstein–Uhlenbeck process - designed so that the mean is our nominal demand, $\mathbb{E}[X_i(t)] = d_i(t)$, and the variance approaches a constant exponentially fast:

  $$\mathrm{Var}(X_i(t)) = \frac{\gamma}{2\alpha}\left(1 - e^{2\alpha t}\right) \tag{12}$$

  The parameters were tuned heuristically to ensure α the mean was respected, and the variance approaches

  $$\mathrm{Var}(X_i(t)) \approx 0.01\mu_i^2 \tag{13}$$

  With μ_i being the mean withdrawal of node i. The noise for each demand is uncorrelated, a conservative approach which ignores geography and climate scales. Implementation on an actual system should be accompanied with data analysis and forecasts to determine realistic noise types for demands.

- Abrupt changes – which we coin *insults* – that occur due to malfunction, weather or other exogenous circumstance. We focus particularly on supply challenges. That is, given a supply profile $s(t)$

  $$s(t) \to s(t) + \Theta(t - T)\Gamma(t) \tag{14}$$

  where Θ is the Heaviside function, T is the time of insult, and Γ is the perturbation. For example, $\Gamma(t) = -s(t)$, simulates a complete loss of supply at time T.

In addition to studying bare "do nothing" scenarios we will also analyze mitigation by controls. We assume that controls at the injection points (off-shore extraction sites at node #1 and node #8 in Fig. 1) and consumption sites, are step-wise. Operationally - due to the close coupling of Israel's gas extraction and delivery - stepwise control is preferable on the supply-side, while significantly idealized for demand nodes.

Focusing on the most challenging cases on fast ramps up (and, possibly, ramps down too) of consumption, e.g. around the time of sundown (or sunrise) in winter, we limit our analysis in this manuscript to *prescribed* control. This allows us to conduct intuitive and easy to interpret tests of possible options. The goal of this exploration is to analyze how the system operator can manage gas transients in line pack, meet power demand evolving throughout a day (or a number of days) while also not exceeding the gas system pressure constraints.

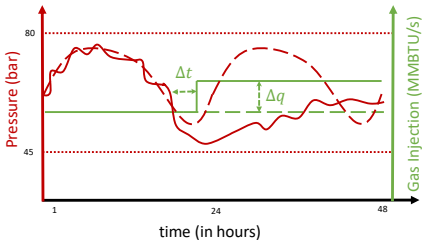

Figure 3: Schematic illustration of the use cases of the system operations during an exemplary period of 48 hours. We show forecasts (long-dashed curves) and actual profiles (solid curves) for a pressure at a node and an injection at an entry point to the system, where a control is applied in response to an insult. See text for details.

Our approach is illustrated schematically in Fig. (3). Long-dashed green curve shows injection profile on one of the entry points to the system. Typically, it is flat where the value (in $MMBTU/s$) is computed based on the balanced forecast of consumption over the entire system and on the operational split of responsibilities between the injection points. Long-dashed red curve illustrates forecast for a pressure at a node of the system. Solid red curve shows an actual pressure profile, which, subject to typical uncertainty, largely follows the forecast till $\approx$ (hour) 23:00, when a significant insult occur and the deviation from the forecast becomes significant. Short-dashed red curves mark node-specific upper and lower limits for the pressure profile. Solid green curve shows operation profile at the injection point, which remains operational (in this use case) through out the 48 hours of observation, however the actual injection profile is not flat – it follows forecast till hour $\approx$ 23:00+Δt when a step-wise control action, responding to the $\approx$ 23:00 emergency, is applied. Selection of the proper time delay Δt, of the control response, and of the respective amplitude, Δq, constitutes a major operational challenge.

The approach to monitoring and prescribed

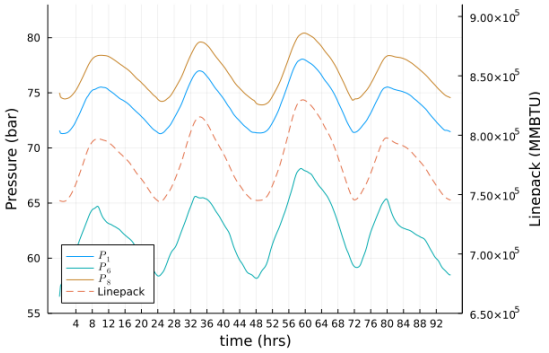

Figure 4: Nominal week in August, with no uncertainty.

control of the system is summarized in Table 1. We present six scenarios of progressive stress. Each scenario is illustrated with a figure summarizing respective dynamics. (Animations of the pressure timeseries across the network, as well as software and data to reproduce all the results included here, can be found at `https://github.com/cmhyett/FluxControlLinepack`.)

We define a pressure crossing as when the nodal pressure falls below 50bar. The survival time τ is defined as the time between initiation of the insult and the time to first pressure crossing *at any node*. Note that due to integrated random fluctuations of demand, we obtain distributions of survival times, shown for example in figure[8] as a shaded region about the median, annotated above with the node at which the pressure crossing occurred. To keep the picture clear, the figures only show pressure crossings for a subset of our nodes, namely 9,1, and 6, as they yield information regarding the north, middle and south of our network respectively.

1. Fig. (4) shows pressures (dashed) and linepack (solid), in a flux-controlled, nominal week in August. It serves as our base case, and importantly, because of the constant flux at supply nodes, the temporal variation of pressure across the network is governed by the intra-day demand fluctuations.

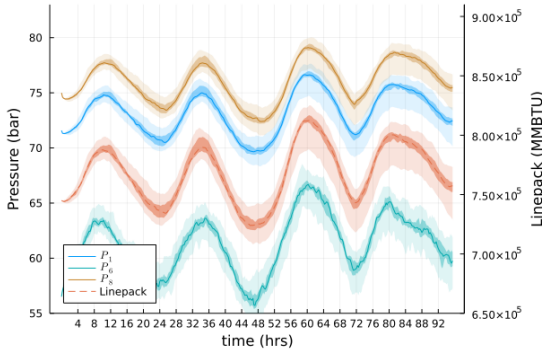

Figure 5: Nominal week in August, with empirical noise added to demand curves. Notice the drift of linepack and pressure jitter, consistent with what was predicted in [7]. Using a Monte-Carlo with 50 simulations, we plot filled regions of containing the middle 75%, 25%, and median using increasing color intensities.

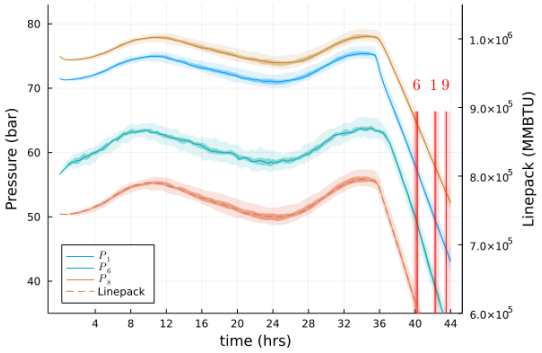

Figure 6: Scenario 3 results, an insult at a crest of the linepack at $t = 36$hrs. Using a Monte-Carlo with 50 simulations, we plot filled regions containing the middle 75%, 25%, and median using increasing color intensities.

2. Fig. (5) adds random fluctuations to demands on this nominal week - modeling uncertainty from exact power demand and generation of renewables. For each node, we add noise distributed uniformly with width of 5% of nominal demand at that node. These small perturbations integrate over time, leading to significant linepack and pressure deviations from the mean.

3. Fig. (6) introduces an "insult" indicating off-nominal or emergency operation. Particularly, supply at node #1 (one of our two supply nodes) are closed at hour 36 in the simulation. We continue to run the simulation to observe the rate of linepack decay and the sequence of pressure crossings. The survival time in this scenario is

$$\tau = 4.13 \pm 0.38 \text{ hrs} \tag{15}$$

where the 0.38 is the standard deviation. This information can be translated to spatiotemporal "vulnerability" of the gas network.

4. Fig. (7) introduces the same insult as scenario 3, but at hour 48 instead of hour 36. In particular, this corresponds to the insult occurring at a trough of the linepack curve instead of a peak. We highlight first that the time to first pressure crossing survival time is shorter in this case

$$\tau = 3.58 \pm 0.89 \text{ hrs} \tag{16}$$

This simple statement that the survival time of the network depends on the start time of an insult is the result of complicated interactions between demand-node boundary conditions as well as network topology.

5. Fig. (8) begins introducing control, attempting to mimic "human in the loop" control of the network under the insult described in scenario 4. In this scenario, the operator at the remaining supply (node 8), increases to the max flow-rate a half hour after the insult begins ($t = 48.5$hrs). This control stabilizes the linepack in the short-term, but fails to handle the daily ramp near hour 60. In particular, the south of the network, far from the remaining supply contains all of

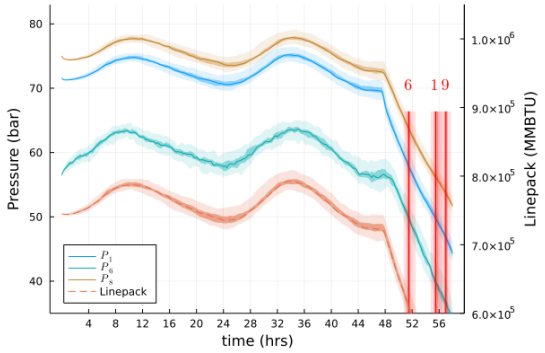

Figure 7: Scenario 4 results, an insult at a trough of the linepack at $t = 48$hrs. Using a Monte-Carlo with 50 simulations, we plot filled regions containing the middle 75%, 25%, and median using increasing color intensities.

the pressure crossings.

$$\tau = 14.17 \pm 4.07 \text{ hrs} \tag{17}$$

6. Fig. (9) finally builds upon scenario 5 to additionally curtail demand 2 hours after the insult ($t = 50$hrs). This translates to a variety of potential action, from high penalty demand-response (as demonstrated during heat waves in California) to the transition of natural gas plants to alternative fuels, or the utilization of stored power.

5 Monotonicity

In our scenario selection, we were intentionally coarse, preferring severe and abrupt challenges, while searching for the mildest controls for remedies. This is intentional, as previous work has given us monotonicity guarantees [8, 9]. That is, we have that for any less-severe challenge (as in the more physically realistic scenario of a slow ramp down of a supply instead of our simulated near-immedate shut off), our pressures will be bounded below by the most severe case, and thus

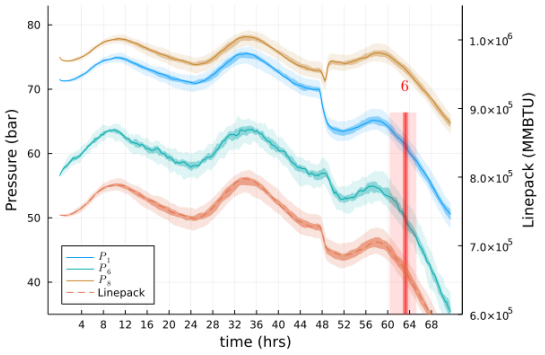

Figure 8: Scenario 5 results, introduces a step-wise increase in supply at node 8 half an hour after the insult ($t = 48.5$hrs).

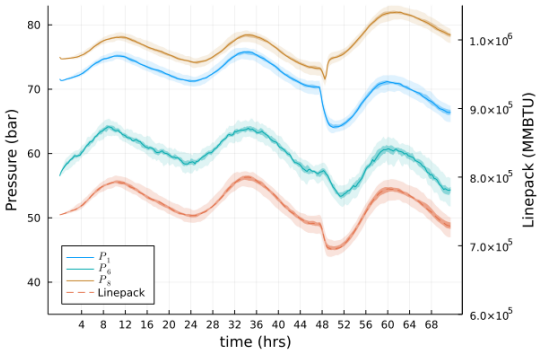

Figure 9: Scenario 6 results, curtails demand at $t = 50$hrs, to maintain minimum pressures across the network.

in turn our estimates for survival times are in fact lower, conservative bounds.

We advocate this approach for schematic expositions as it is only with full operational and procedural knowledge that one can obtain tight estimates - that is, work inherently reliant on proprietary data.

It should also be noted that monotonicity can yield bounds for the more usual scenario of pressure and linepack drift resulting from integration of stochasticity due to renewables, such drift can be seen in Fig.5. However, monotonicity bounds were derived without relation to probability, thus it is likely that future work can tighten these bounds, avoiding expensive simulation except when full distributional knowledge is needed.

6 Conclusion

We investigate the spatiotemporal response of a reduced model of Israel's NG network to prescribed insults and human-in-the-loop controls in order to evaluate robustness and suggest control strategies. To reiterate, Israel's network is unique because of the absence of a compressor, and that the inlets specify flux, not pressure. Further, we perform this study looking towards the increased importance of NG to mitigate increasing stochasticity in demands expected in the coming years as coal is phased out, and renewables grow.

The specification of flux vs pressure leads to the pressure timeseries of the network being dominated by daily demand curves as shown in Fig. (4), increasingly susceptible to pressure drift from stochastic fluctuations in nominal demands.

Further, we call out the importance of robustness of the network not simply to insults, but to insults at any time - leading to the idea of "system reserve" being time and spatially dependent.

Future work will improve on modeling to more completely capture uncertainty propagation through the network, and its influence and interaction with control strategies. We envision extending the prescribed control, also reinforced by monotonicity [8, 9], developed in this manuscript with the powerful optimization approaches developed to account for dynamic optimization over compressors [10, 11, 12, 13, 14], e.g. to evaluate benefits of adding compressors to the NG system of Israel. We also plan to carry on a comprehensive modeling and control of the combined power and gas system of Israel, in the spirit of the approach highlighted in [15, 16].

Acknowledgments

The authors are grateful for discussions with Anatoly Zlotnik, Vitaliy Gyrya, and Kaarthik Sundar. CH, LP and MC acknowledge support from UArizona, as well as travel grant from NOGA Israel. CH acknowledges support from NSF's Data-Driven Research Training Grant.

References

[1] A. Osiadacz, "Simulation of transient gas flows in networks," *International Journal for Numerical Methods in Fluids*, vol. 4, pp. 13–24, Jan. 1984.

[2] M. C. Steinbach, "On PDE solution in transient optimization of gas networks," *Journal of Computational and Applied Mathematics*, vol. 203, pp. 345–361, June 2007.

[3] M. Chertkov, S. Backhaus, and V. Lebedev, "Cascading of fluctuations in interdependent energy infrastructures: Gas-grid coupling," *Applied Energy*, vol. 160, pp. 541–551, 2015.

[4] V. Gyrya and A. Zlotnik, "An explicit staggered-grid method for numerical simulation of large-scale natural gas pipeline networks," *Applied Mathematical Modelling*, vol. 65, pp. 34–51, 2019.

[5] K. Sundar, "GasTranSim Julia package." `https://github.com/kaarthiksundar/GasTranSim.jl`, 2008.

[6] E. S. Menon, *Gas Pipeline Hydraulics*. CRC Press, 2005.

[7] M. Chertkov, V. Lebedev, and S. Backhaus, "Cascading of Fluctuations in Interdependent Energy Infrastructures: Gas-Grid Coupling," Nov. 2014. arXiv:1411.2111 [physics].

[8] M. Vuffray, S. Misra, and M. Chertkov, "Monotonicity of dissipative flow networks renders robust maximum profit problem tractable: General analysis and application to natural gas flows," in *2015 54th IEEE Conference on Decision and Control (CDC)*, pp. 4571–4578, 2015.

[9] A. Zlotnik, S. Misra, M. Vuffray, and M. Chertkov, "Monotonicity of actuated flows on dissipative transport networks," in *2016 European Control Conference (ECC)*, (Aalborg, Denmark), pp. 831–836, IEEE, June 2016.

[10] H. H. Rachford, Jr. and R. G. Carter, "Optimizing Pipeline Control In Transient Gas Flow," pp. PSIG–0004, Oct. 2000.

[11] R. G. Carter and H. H. Rachford, Jr., "Optimizing Line-Pack Management to Hedge Against Future Load Uncertainty," pp. PSIG–0306, Oct. 2003.

[12] H. H. Rachford, Jr., R. G. Carter, and T. F. Dupont, "Using Optimization In Transient Gas Transmission," pp. PSIG–0903, May 2009.

[13] A. Zlotnik, M. Chertkov, and S. Backhaus, "Optimal control of transient flow in natural gas networks," in *2015 54th IEEE Conference on Decision and Control (CDC)*, (Osaka), pp. 4563–4570, IEEE, Dec. 2015.

[14] A. Zlotnik, M. Chertkov, R. Carter, A. Hollis, A. Daniels, and S. Backhaus, "Using Power Grid Schedules in Dynamic Optimization of Gas Pipelines," pp. PSIG–1612, May 2016.

[15] *Impact of Regulatory Change to Coordinate Gas Pipelines and Power Systems*, vol. All Days of *PSIG Annual Meeting*, 05 2016. PSIG-1611.

[16] A. Zlotnik, L. Roald, S. Backhaus, M. Chertkov, and G. Andersson, "Coordinated scheduling for interdependent electric power and natural gas infrastructures," *IEEE Transactions on Power Systems*, vol. 32, no. 1, pp. 600–610, 2017.

Appendices

Author Biographies

Criston Hyett - is a Ph.D. student in Applied Mathematics at the University of Arizona. He is advised by Misha Chertkov, and interested in data-enhanced dynamical systems modeling, encompassing physics-informed machine learning, reduced order modeling and uncertainty quantification.

Laurent Pagnier - is a Visiting Assistant Professor at the University of Arizona. His main research interest is the application of Machine Learning techniques to the operation of large infrastructures. He is particularly interested in reinforcing the interpretability and trustworthiness of ML methods which are paramount to increase their acceptance and usage by practitioners.

Jean Alisse - received his Phd in Physics in 1999 (Paris University). He worked during 11 years at the Israel Electric Company in the Planning and Division company. There he headed a Modeling group which focused on CFD problems and Natural Gas dynamics. Since the creation of Noga, the Israel Independent System Operator, he has been pursuing the same works, with a stress on developing models for Gas dynamics simulation and Gas-Power systems.

Lilach Sabban - received her PhD from the Technion Israel Institute of Technology. Lilach specializes in fluid dynamics as a mechanical engineer. She is a researcher at Noga, Israel Independent System Operator, involved in a range of

Scenario #	Description	Features
1	A reference week in August.	Pressure variation in flow-control regime
2	Scenario #1 with empirical noise added to demand curves, supplies unchanged.	Linepack and pressure drift when using flow-control with uncertain demand.
3	Scenario #2 with insult at node 1.	Introduce the notion of survival time, and set baseline without any controls.
4	Scenario #3 with insult time change to trough of linepack timeseries.	Illustrate that survival times change with timing of insult.
5	Scenario #4 with step-wise supply increase from node # 8.	Survival times lengthen, but become less certain.
6	Scenario #5 with step-wise curtailing of demand.	No low pressure crossings are found. The high pressure at node # 8 shows need for finer control.

Table 1: Description of scenarios.

renewable energy projects and has been investigating natural gas dynamics.

Igal Goldshtein - received his B.Sc from the Technion Israel Institute of Technology. He worked at Israel electric company for 12 years, seven of them as Gas-Turbine dispatcher in the system operator control center. During the last two years, at Noga, the Israel System Independent Operator, he handles the Operator Training System (OTS). He also researches operation of Israel electric system under various stress conditions.

Michael (Misha) Chertkov - is Professor of Mathematics and chair of the Graduate Interdisciplinary Program in Applied Mathematics at the University of Arizona since 2019. He focuses in his research on foundational problems in mathematics and statistics applied to physical systems, in particular fluid mechanics, to engineered systems such as energy grids, and to some bio-social systems. Dr. Chertkov received his Ph.D. in physics from the Weizmann Institute of Science in 1996, spent three years at Princeton University as a R.H. Dicke Fellow in the Department of Physics, and joined Los Alamos National Laboratory in 1999, initially as a J.R. Oppenheimer Fellow and then as a Technical Staff Member in Theory Division. He has published more than 250 papers, is a fellow of the AAAS, a fellow of the American Physical Society and a senior member of IEEE.